Mario Navarro González

Design and implementation of a functional SSVEP-based Brain Computer Interface

Final Degree Project

Directed by Alfonso Romero Nevado

Bachelor's Degree in Telecommunication Systems and Services Engineering

UNIVERSITAT ROVIRA I VIRGILI

2024

Here is an area of great confusion
Here is a section that’s extremely precise
Here is a connection with the opposite side

David Byrne

Acknowledgements:

Many thanks to all the people who collaborated and believed on some way on this project, I would like to thank to Dr Luis Martinez Salamero for the advices and the books on the matter of the analog signal processing.
To Dr Hatem Rashwan and Dr Roger Guimerà for their generosity and availability on advising me on the predictive algorithm.
And of course, to my director, Dr Alfonso Romero whose guidance and freedom on the decisions of the project has been game-changing and enjoyable.

To my parents for supporting me in every aspect of my life and education.
And then last but not least to my partner whose unconditional support and motivations on me has been essential the whole process.

Table of content

Table of Figures:

Table of Equations

Table of tables

Abstract

In the present project, a new Electroencephalogram (EEG) Brain Computer Interface (BCI) has been implemented, the BCI is Steady State Visual Evoked Potential (SSVEP) based, namely, when the user stares to an objective that is blinking at a defined frequency, this same frequency should appear on the spectrum of the EEG when measuring on the occipital lobe.

The circuit has been designed and made using Sallen-Key Filters, Amplifiers and the Arduino MKR1010 microcontroller. It has also been tested an implemented a self-new algorithm for the detection of the correct SSVEP frequency.

Resumen

En este proyecto, se ha implementado una Interfaz Ordenador-Cerebro basado en SSVEP, es decir, cuando el usuario mira fijamente a un objetivo que parpadea a una frecuencia determinada, esta misma frecuencia debe aparecer en el espectro del EEG cuando se mide en el lóbulo occipital.

El circuito se ha diseñado y fabricado utilizando filtros de Sallen-Key, amplificadores y el microcontrolador Arduino MKR1010. También se han probado distintos algoritmos y se ha implementado un nuevo algoritmo propio para la detección de la frecuencia SSVEP correcta.

Keywords

SSVEP, Brain Computer Interface, EEG, Analog Signal Processing, Digital Signal Processing.

Introduction

Motivations

The motivation for doing this project comes with the interest of the author on the matter, both from the three main branch's on the project, the first one the EEG signals and the neurological mysteries. The second main branch, the analog signal processing and the last one, the digital signal processing and the delivering a final product. All of them with an important component of innovation.

BCIs is the forefront of the actual research on the neuroelectric field. Being able to detect and interpret EEG signals and also to stimulate some regions as a treatment are the main purposes.

It has been more than fifty years since the first BCI [1], and it's still being investigated and having new discoveries like the implantation of Neuralink first chip.

Theoretical Framework

Historical context

It is widely known that the human body can be considered a machine, even the great philosopher René Descartes said so on 1637:

"Every body is a machine, and the machines made by the divine craftsman are the best made, without, however, ceasing to be machines. If we consider only the body, there is no difference in principle between the machines made by men and the living bodies created by God. The only difference is one of perfection and complexity." [2]

As all the machines we know it works with energy, and this energy is in form of electrochemical and electrical fields and electrical currents through the neurons systems on the brain, all these electrical activities can be recorded with the same systems and sensors (Adapted) that could be used on measuring other machines.

In fact, this year marks the 100th anniversary of the invention of the EEG system by Hans Berger, every year following, the EEG has been used to diagnose

illnesses like schizophrenia, until 1977 when Dr. Jacques Vial developed the first Brain Computer Interface with visual evoked potentials.

Although most of the papers on the matter uses premade analog systems, and other ones uses premade digital systems, It has been found that in 2018, Ronan Byrne [3] aimed to do a full BCI system on his Thesis, but despite that the circuit and the digitalization of the signal was performed, the final implementation with a fully working ecosystem was not accomplished.

Driven Right Leg Circuit

The Driven Right Leg (DRL) circuit is a widely used circuit on the field of EEGs and BCIs. This circuit uses the common mode voltage of the instrumental amplifier and drives it back to the subject acting as a feedback electrode placed on the ear lobe to reject the maximum number and power of interferences.

SSVEP signals

The Steady-State Visual Evoked Potential is a signal-event that occurs on the occipital lobe when the subject stares at a flickering objective, it has been proved that the flickering frequency and it's harmonics appears on the EEG spectrum. This spectrum generally has a bandwidth of 0.01 Hz to 100 Hz, inside this bandwidth all mostly known EEG waves are found, and so SSVEP signals which has a small portion of this bandwidth: from 6 Hz to 30 Hz. All the general bandwidth partition can be seen on Figure 1.

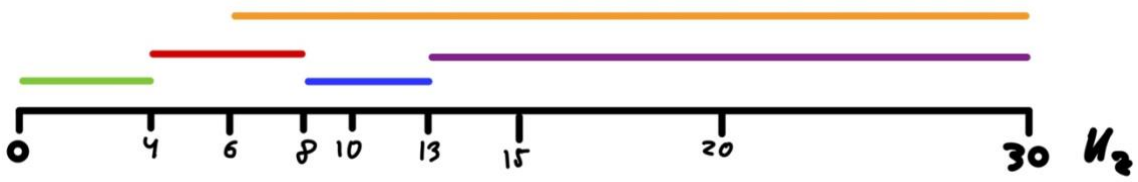

Figure 1. EEG general bandwidth where green stands for Delta Waves, Red for Theta Waves, Blue for Alpha Waves, Purple for Beta Waves and Oranges shows the medium and higher bands of the SSVEP signals.

Because of the overlapping with alpha waves, the first stimulus frequency that has been chosen is 10 Hz, the other one is 15 Hz which is one of the highest flickering frequencies that is typically used.

It has been found that SSPVEP signals are periodical (during the stimulation at a given frequency), this feature enables the possibility of detecting the signal searching its frequency without any training of the subject.

Other methods or events like Visual Evoked Potential or P300 signals are harder to be detected and need training of the subjects.

Objectives

The main objective of the project is:

- To be able to predict which pulsating objective is being observed between two possibilities with a self-made analog circuit and a self-made software.

The secondary objectives are:

- To be able to detect and represent brain waves on the oscilloscope.
- To develop a fully working one-channel EEG systems that could process brain signals with an analog circuit.
- To digitalize this signal with a common microcontroller.
- To process digitally the signal to obtain the desired features.
- To predict which objective is being observed.
- To record the performance of the system with two widely used parameters.

Methodology

Hardware: Analog Signal Processing

The main schematic of the hardware can be checked on the blocks diagram on Figure 2.

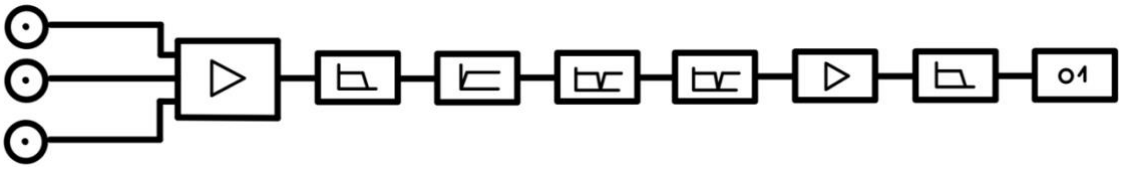

Figure 2. General Block Diagram of the Hardware System

Signal sensing

It is known that there are two main types of electrodes, dry electrodes and wet electrodes, in this project the electrodes that were chosen were the wet ones because of its low-cost price, the easy-to-use characteristic, and the better signal to noise ratio in comparison with dry electrodes [4], these electrodes can be seen on Figure 3. And the specific model can be found on the budget annex.

Figure 3. Electrodes from DORMO used on the project.

At the first stages of the project the electrodes were connected to the circuit with some alligator clips and later on the development with the specific clips that can be checked on Figure 4. The specific model can be found on the budget annex.

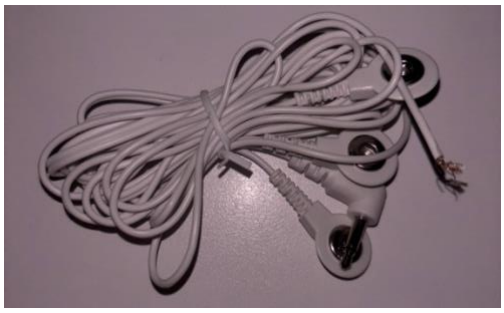

Figure 4. TEM cables used on the project.

Because of the low-cost condition of the project, those clips were not specific for EEG acquisition, they were aim for other techniques like electrostimulations for physician's therapy.

However, to demonstrate that the wiring between the electrodes and the amplification stage do not affect the quality of the signal, some proves were made. The main schematic of the experiment can be checked on Figure 5 and Figure 6. It consisted of a signal generator which is a PCB that is power with a 9V battery, an oscilloscope and the electrode wiring.

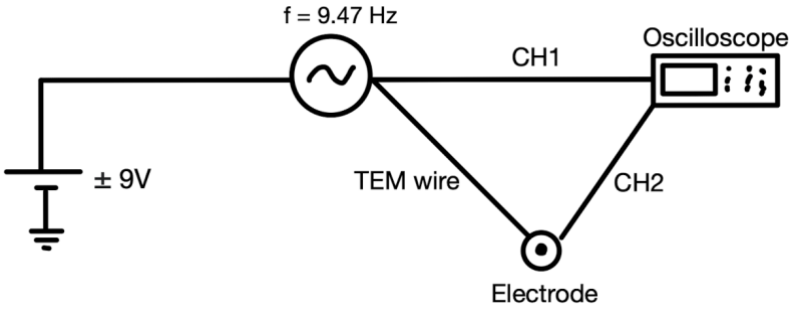

Figure 5. General Assembly of the Signal Integrity Test.

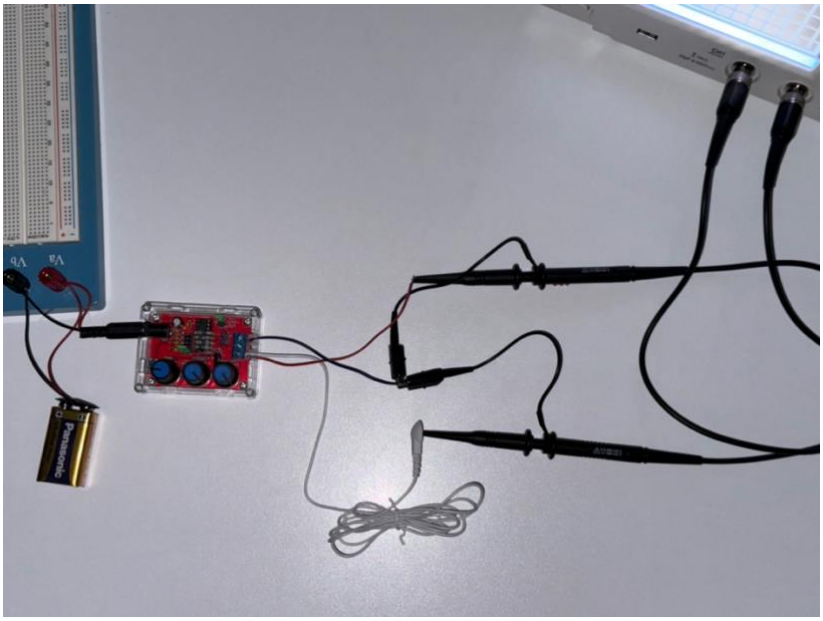

Figure 6. View of the Signal Integrity Test assembly.

The signal generator made a signal of 9.47 Hz which is inside the frequency band of the SSVEP, this signal generator is connected with one channel of the oscilloscope and also connected to one side of the wire, while the second channel of the oscilloscope is touching the other side of the wire. Then the comparison between the input and the output of the wire can be observed in Figure 7. The signal does not present any type of attenuation or frequency shift.

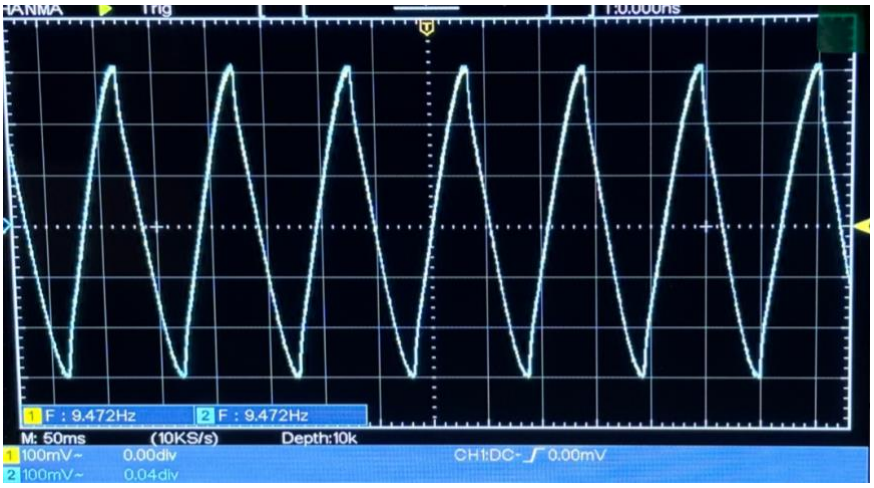

Figure 7. Result of the Signal Integrity Test.

In order to remain within the scope of work the decision of making the BCI of only one channel was taken. Namely, for one channel, three electrodes must be used, two for the differential signal and the other one for the driven right leg that will be used as a reference.

The placement of the electrodes follows the 10/20 [5] system, and are placed on the occipital lobe, specifically at O2 and O1.

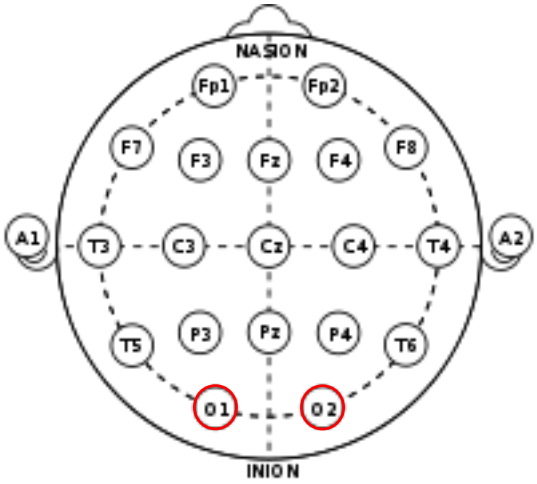

Figure 8. 10/20 Electrodes placement System. [6]

In summary, wet electrodes were used and placed on the mastoid part of the temporal bone for the driven right leg input and the occipital lobe for capturing the SSVEP signal. Moreover, the TEM cables were chosen for the prototype.

Amplifier Stage

It is widely known that the first element in a chain must have the higher gain and lower noise. For this application a high gain must be accomplished because of the low level of the signal (being approximately at microvolts) this signal should be amplified until almost some millivolts, for being detectable for the digitalization process. Also another important feature that the amplifier must have is to have a port for the driven right leg to have an electrode of reference that will be placed on the mastoid part of the temporal bone in order to reject the common mode.
It has been used a pre-made instrumental amplifier from the electronics laboratory from URV, Figure 9.

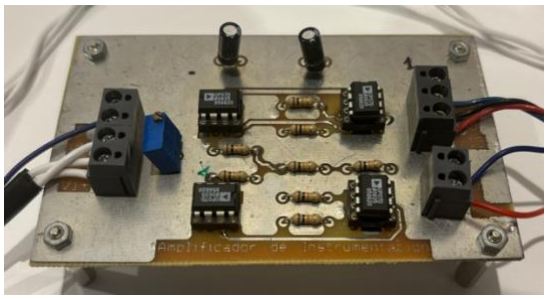

Figure 9. Instrumentation amplifier

The inputs and outputs of the circuit are three, the first one is the power, composed by the positive voltage (+ 9V with the batteries), the negative voltage (- 9V) and the ground. The other input contains the connections to the electrodes, namely, the O2 and O1, the driven right leg and a ground. Finally, the circuit has one output in which there are two wires, one for the amplified signal itself, and the other one with the ground.
For this circuit the operational amplifiers that were used were OP27G from Texas Instruments [7].

Active Low Pass Filter

Once the signal has been amplified, the filtering stage has to be implemented, it can be summarized in one bandpass filter and some notch filters for rejecting the main power interface and its harmonics.

For choosing the right cutting frequencies, there is a need of knowing the bandwidth of the brain activity and the bandwidth of the target frequencies (SSVEP), as it has been proved some pages early, the frequency band of the brain is between 0.01 Hz and 100 Hz. While the SSVEP frequencies goes between 8 Hz to 30 Hz. The analog filter is intended to make the bigger frequency cut, letting pass all the frequencies of the brain bandwidth and the DC component, while later, the digital filter will spin a finer yarn on the SSVEP bandwidth.

As humans can be considered like some type of receiving antennas [8] there are a lot of undesired signal interferences of higher frequency than our bandwidth (of some kHz or MHz) that the analog LPF must delete.

Specifically, a Sallen-Key LPF was designed and implemented with a cut frequency of 106 Hz. The transfer function of the LPF can be found on Annex 1 which leads to the equation that defines the cutting frequencies which is (Equation 1)

$$fc = \frac{1}{2\pi * \sqrt{R1 * R2 * C1 * C2}}$$

Equation 1. Cut Frequency of a Sallen Key Low Pass Filter.

The general Sallen-Key LPF circuit can be seen at Figure 10.

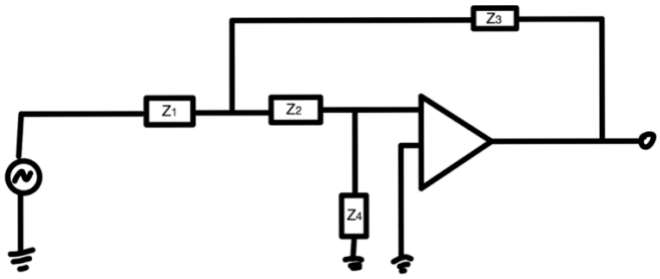

Figure 10. Sallen Key Low Pass Filter whose values are: Z1 = 1.5 kΩ, Z2 = 1.5 kΩ, Z3 = 1µF, Z4 = 1µF.

Then, with the Okawa-Denshi [9] program, the bode diagram (Figure 11) is computed to proof that the frequencies of interest are inside the passing zone.

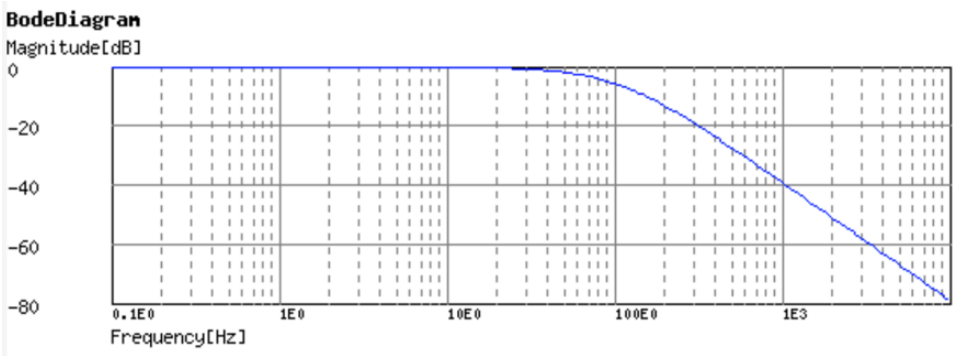

Figure 11. Bode Plot of the Low Pass Filter.

Active High Pass Filter

Even the major frequency band is considerably low (less than a centenar Hertz's) there is a need of implementing an active HPF for the mitigation of the DC component. It is important to take into account that all of the active components add some offset error, because of the low-cost variable. But the active HPF takes almost all the DC. In this case, the cutting frequency should be really low in order to avoid attenuation at the interesting bands. So, it was fixed to fc = 0.01 Hz, this implies really high values of resistances. As with the LPF, this filter has it's transfer function is demonstrated on the Annex 1, and it's result and cutting frequency is defined on equation 2.

$$fc = \frac{1}{2\pi * \sqrt{R1 * R2 * C1 * C2}}$$

Equation 2. High Pass Filter cutting frequency.

And in this case, the topology of the system changes as it can be checked on figure 12, at the place of the resistances there are now capacitors and vice-versa. As mentioned previously, the resistances have high values, and the desired value is accomplished with relationships between resistors.

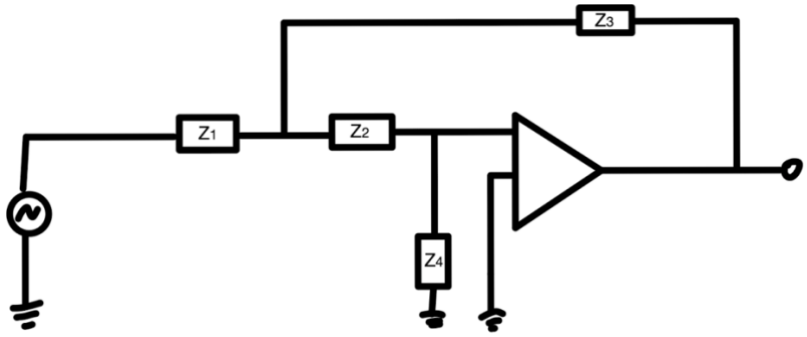

Figure 12. Sallen Key Low Pass Filter whose values are: Z1 = 1 µF, Z2 = 1 µF, Z3 = 15.9 MΩ, Z4 = 15.9 MΩ.

So, the non-commercial values of Z3 and Z4, will be accomplished with the summation of R1 = 10 MΩ, R2 = 4.7 MΩ, $R3 = 1.2\ M\Omega$.

Then, with the Okawa-Denshi [9] program, the bode diagram (Figure 13) is computed to proof that the frequencies of interest are inside the passing zone.

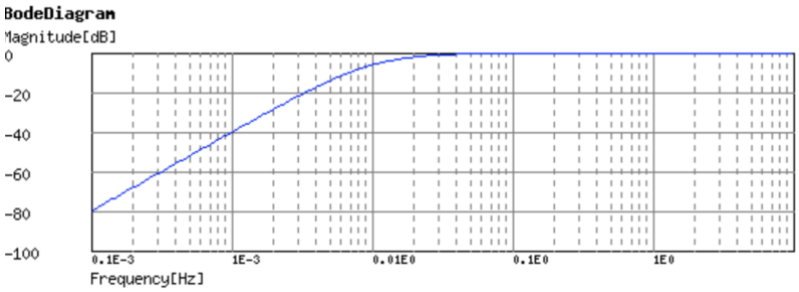

Figure 13. Bode Plot of the High Pass Filter.

Active Notch Filter 50 Hz

After the general bandwidth is selected, it is important to know all the interference inside it, the most important is the main power interference which is at 50 Hz (in the case of Europe) and its harmonic at 100 Hz.

At a first approach, a passive doble twin t was implemented, but because of the high amplitude of the interference, it was found the need of having an active circuit (Figure 14). [10]

$$f_{notch} = \frac{1}{2\pi * R * C}$$

Equation 3. Cutting Frequency of the Active Notch Filter.

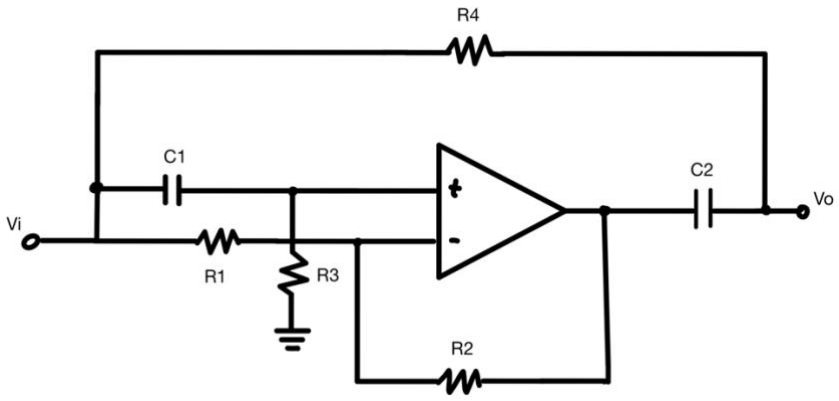

Figure 14. Active Notch filter at fc = 50 Hz, the values for this circuit: R4 = R3 = 68kΩ ; R1 = R2 = 10kΩ ; C1 = C2 = 47 nF.

Passive Notch Filter 100 Hz

Because of the high amplitude of the main power interference, the first harmonic (at f*2, 100 Hz) is also quite relevant, and if it is not processed it could mask the EEG signal. The purposed circuit is much simpler than the Active Notch Filter, it consists of a typical and widely used Twin-T notch [11] filter as it can be checked on Figure 15.

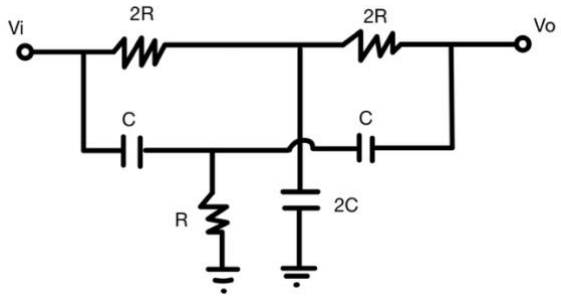

Figure 15. Passive Notch Filter on the main power harmonic interference.

The cutting frequency is defined at Equation 4 which leads to the values of R = 11.7 kΩ and C = 68 nF.

$$f_{notch} = \frac{1}{4\pi * RC}$$

Equation 4. Cutting frequency of the Passive Notch Filter.

Hardware: Signal Conditioning and Digitalization

Passive Low Pass Filter

Once the signal was cleaned enough, the signal conditioning stage began. First of all, a passive RC Low Pass Filter was implemented at a frequency of 60 Hz, namely, a resistance of R= 47 KΩ and a capacitor of C = 1 μF.

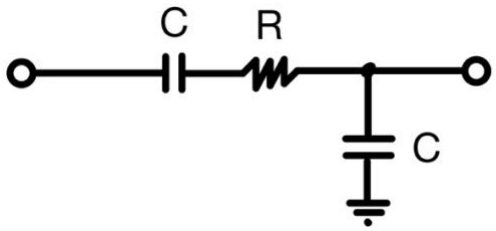

Figure 16. Passive Low Pass Filter.

$$f_c = \frac{1}{\pi * RC}$$

Equation 5. Cutting Frequency of the Low Pass Passive Filter.

Voltage Divider

There is an independent circuit to the acquisition one, it consist in a voltage divider whose schematic can be checked on Figure17. The aim of this circuit is to get a fix and constant voltage of approximately 1 Volt to make it the Analog reference for the microcontroller. The power supply in this case is an output of the microcontroller itself (to avoid any fluctuation on the reference). In deep, the power supply is 5 volts and the resistance values are obtained with the general equation of the voltage divider (Equation 6).

$$V_o = V_i * \frac{R_2}{R_1 + R_2} \quad ; \quad R_1 = 4 * R_2$$

Equation 6. Voltage Divider Equation.

Which leads to a R1 = 2.2 kΩ , and a R2 = 1 kΩ. With the multimeter is checked that the Vo is 1.5V.

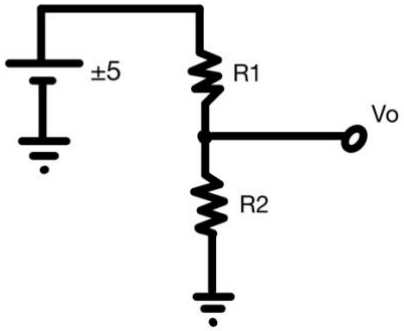

Figure 17. Voltage Divider Assembly for the Analog Reference.

Microcontroller

The microcontroller used in the project was the Arduino MKR1010 [12] because of the size, price and the feature of the ADC converter which can be configured to work at 12 bits. And whose analog reference can be changed from 5 V to an external voltage value which in this case is the output of the voltage divider (~1.5 V). The sampling frequency of the system is approximately fs = 1105 Hz.

Hardware: Final Prototype

Firstly, the system was assembled on a testing protoboard that can be seen on Figure 18.

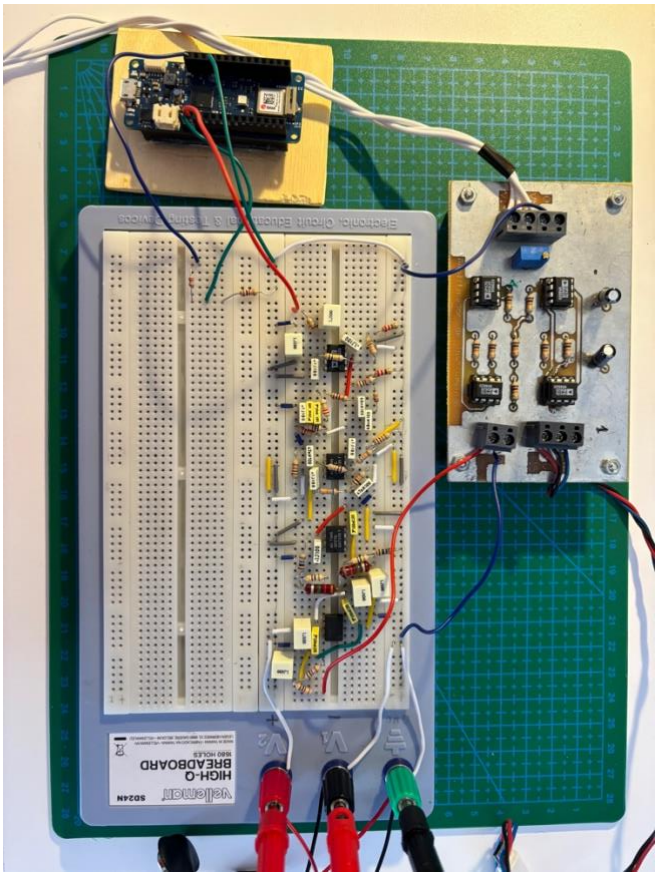

Figure 18. Full working system on the testing protoboard.

Then the system was ready to be soldered into the holes plate. In order to be sure that the system was conserved, all the components were acquired for duplicated in order to maintain the testing protoboard always working.

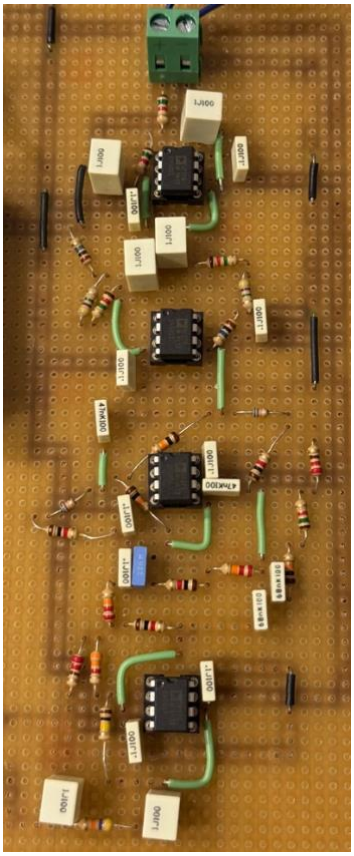

Figure 19. Analog Signal Processing on the soldered Protoboard.

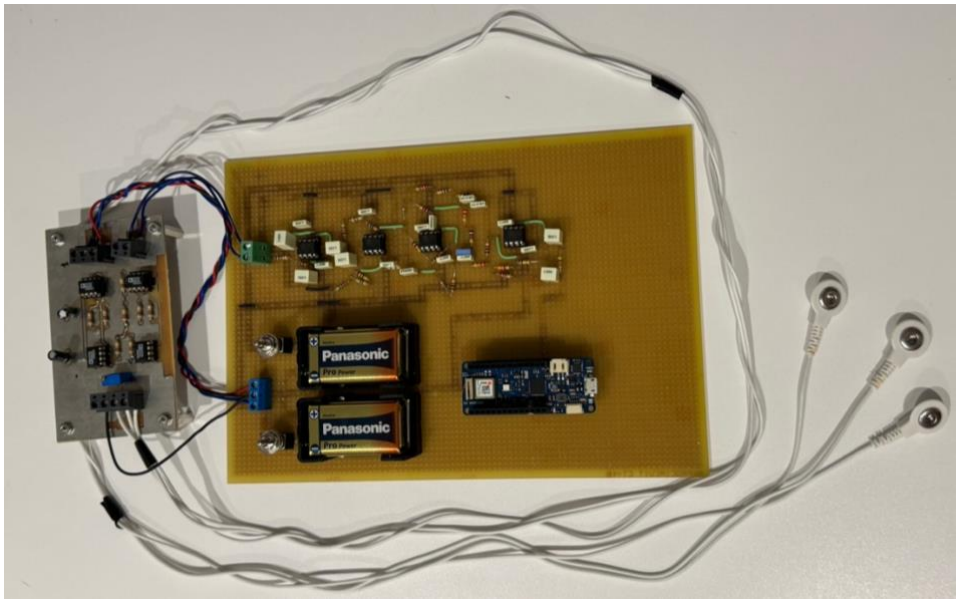

Figure 20. Full Soldered system.

Figure 21. Power of the circuit, levers for the activation and the microcontroller, Arduino MKR1010.

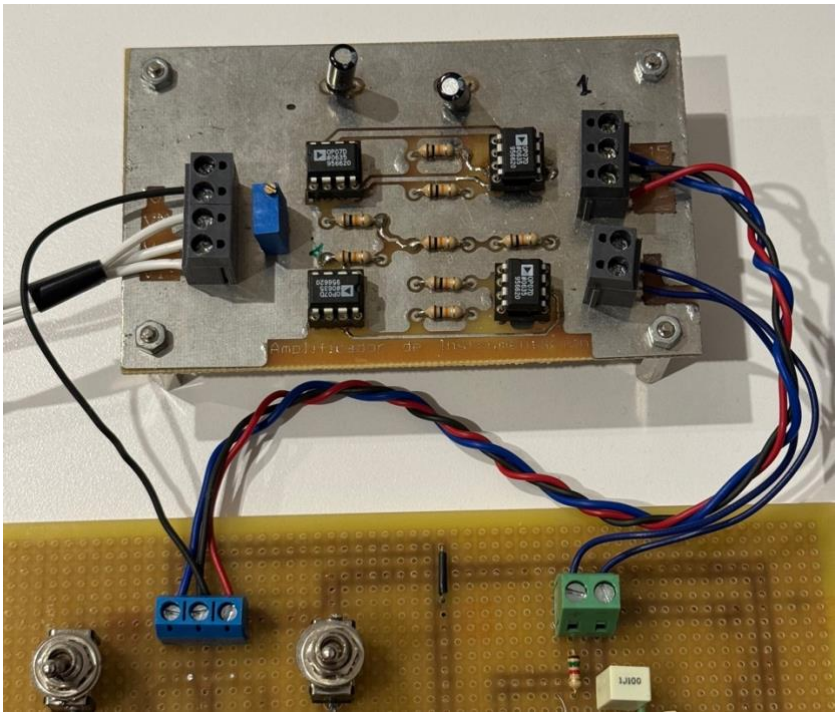

Figure 22. Instrumental Amplifiers.

Software

The software can be divided in three different parts, the first one is for making the blinking page, where two different objectives are placed on a black screen, each of them blinks at a different frequency which is inside the bandwidth of the SSVEP signals. Then the other code gets and plots all the data acquired by the hardware system, there are several representations that can be made. Inside the Visualizer interface there is the result of the prediction. But many different tests were performed to discover which was the algorithms that fits the most on the system.

Blink

The blink code was tried on Python but led to some error and randomness on the blinking frequencies. Then, the decision of making the program on JavaScript and HTML was taken. This programming language was chosen because of the support on the animations of it. On the HTML code, both squares were defined while on the JS code the animation was coded, it consisted of a function for changing the background color of the square from white to black, and a setInterval function that works with an input period of time, that can be computed with the inverse of the blinking frequency. Then for an analytical demonstration over the blinking frequency a new method for counting the time between execution was implemented. And the result of it can be checked on Figure 23.

Figure 23. Result of the testing frequencies.

In order to reduce this error, it was found that the program has better performance on Safari than on other searchers like Google Chrome or Mozilla Firefox. Finally, the full view can be seen on Figure 24.

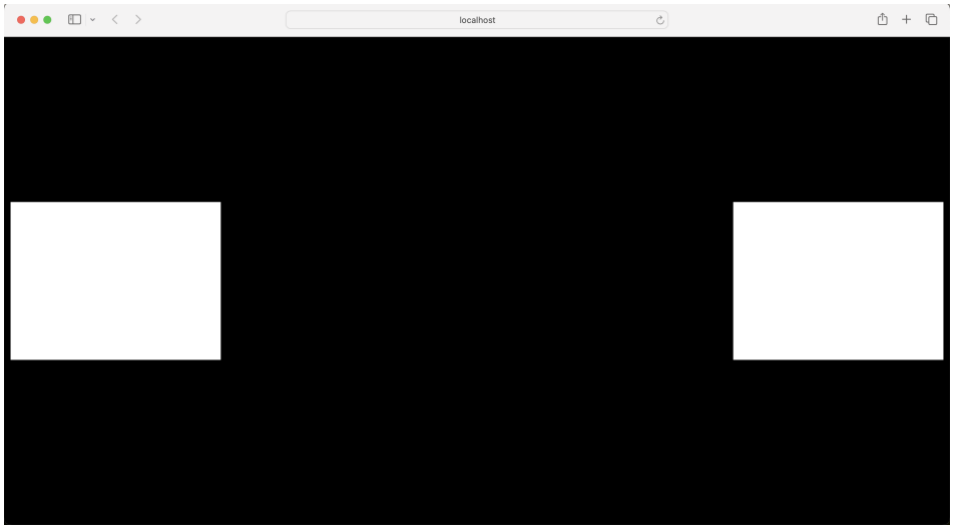

Figure 24. Main view of the Blink Program.

Visualizer

The visualizer program is the biggest code on the project. It makes a triple function, as it receives the data, plots it and shows the predictions. This interface was made with the library PyQt5. The result can be seen on figure 25.

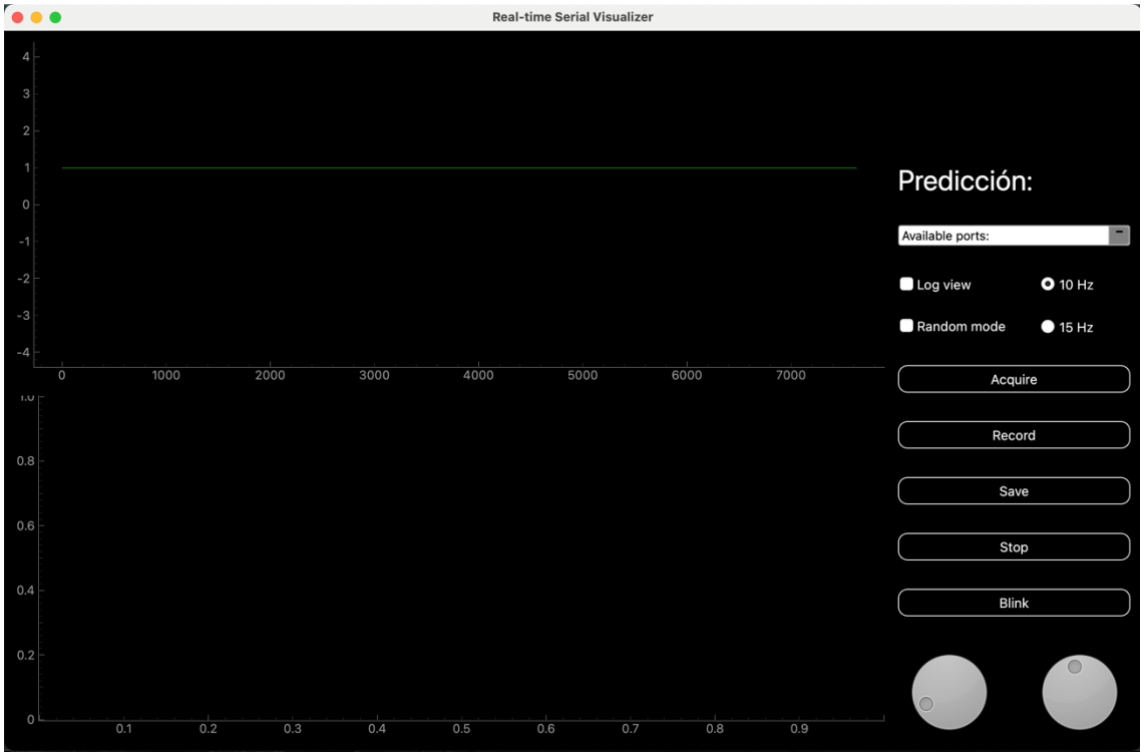

Figure 25. Final View of the Visualization program without any input.

On the left side we can found two graphs, the first one is for the temporal signal, when a sample is added on the right part of the graph, a sample is popped on the left side. Then on the lower side there is a representation of the Power Spectral Density which is the variable that is used to get the prediction. Then on the right side of the screen there are several controllers in order to help on the visualization. From top to bottom there is the resulting prediction, the drop-down for selecting the port (if there is no port selected an error message appear to the user) Figure 26,

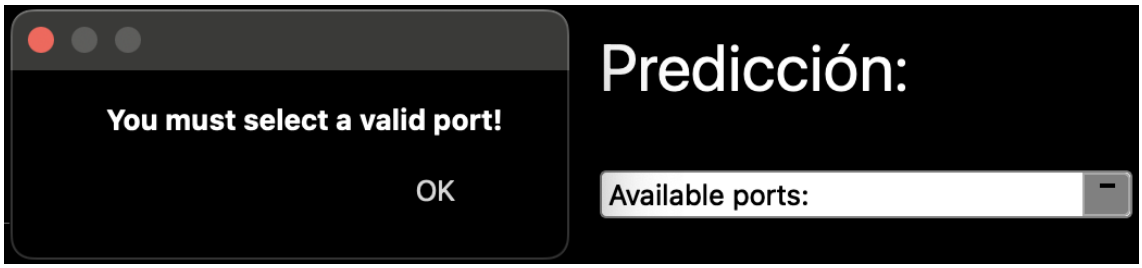

Figure 26. Error Message if no port is selected.

next there are the check buttons for getting the PSDA on a logarithmic point of view and the random mode which is used for testing.

Then, a series of buttons are available for the user to record or save the signal, the "Acquire" button begins the acquisition of the serial port, then the "Record" button is for start saving the samples, the "Save" button is used for stopping the record function and to save to csv the data recorded, the "Stop" button is used for stopping the acquisition began with the acquire button. Finally, the Blink button, that gives the user access to the blink program.

Finally, there are two dials that can be used to change the scale of the time graph and the PSD graph, but this option is not recommended because it has been studied which is the better window time. On figure 27 it can be found how the Visualizer looks with the Arduino connected but the power of the analog circuit is off and the electrodes are not placed. Moreover, on figure 28 it can be seen the fully working system and the EEG signal.

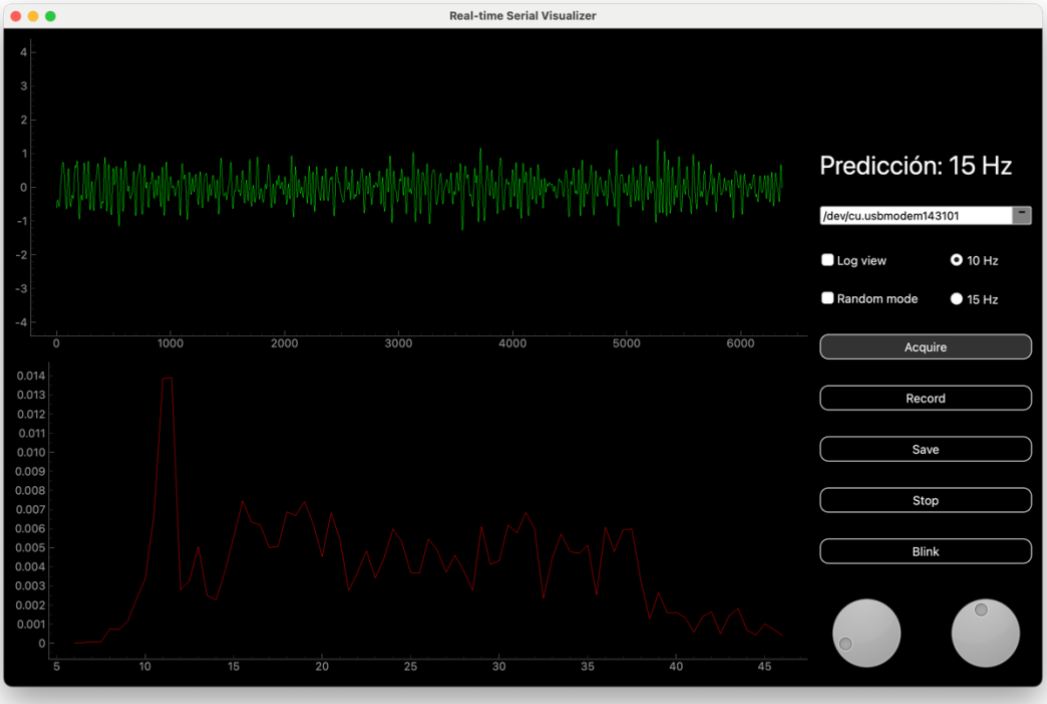

Figure 27. Analog entry of the Arduino with no electrodes placed and the circuitry without power.

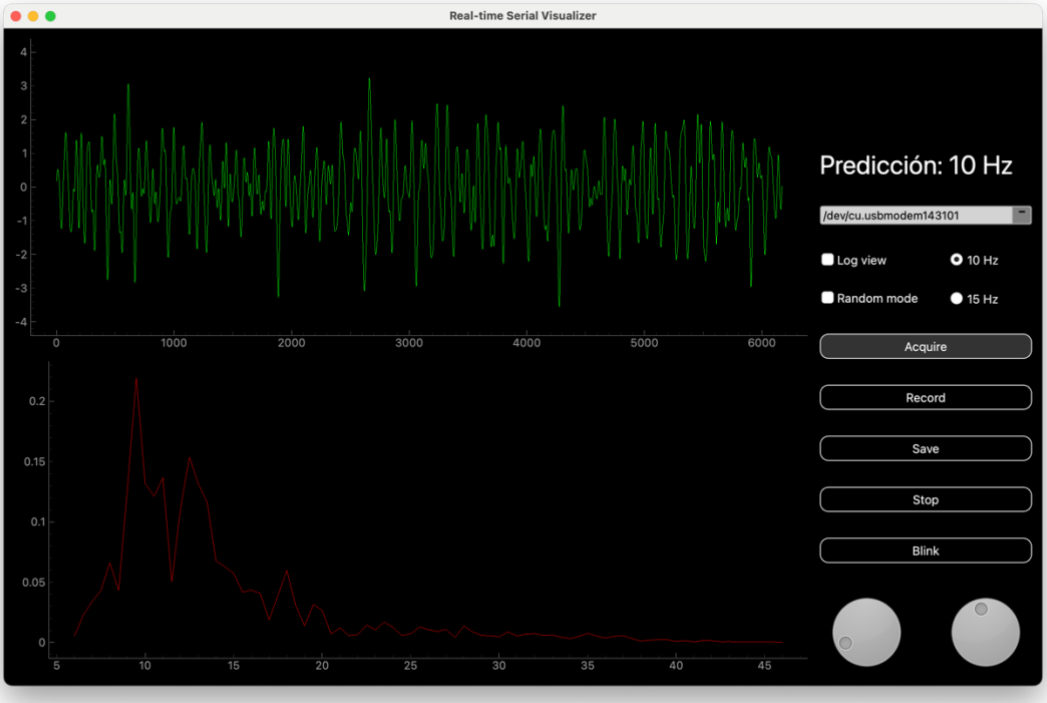

Figure 28. Fully working acquisition system gazing at a 10 Hz stimulus.

Digital signal processing

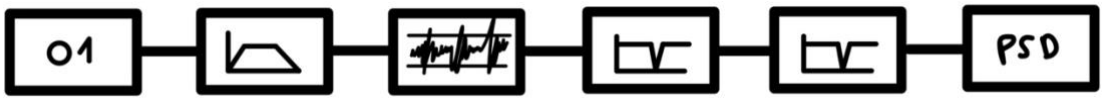

Figure 29. Block Diagram of the Digital Signal Processing.

Some digital signal processing was applied in order to increase the accuracy of the system. First of all, as the buffer (the window time) of the signal is full, a Butterworth bandpass filter is applied with a low cutting frequency of 7 Hz and a High cutting frequency of 40 Hz. This is approximately the bandwidth of the SSVEP signals. Although in this project, one objective is blinking at 10 Hz and the other one at 15 Hz (which leads to a bandwidth of 10 Hz to 30 Hz (which is the second harmonic of 15 Hz)). The bode plot of this digital filter can be checked on Figure 30.

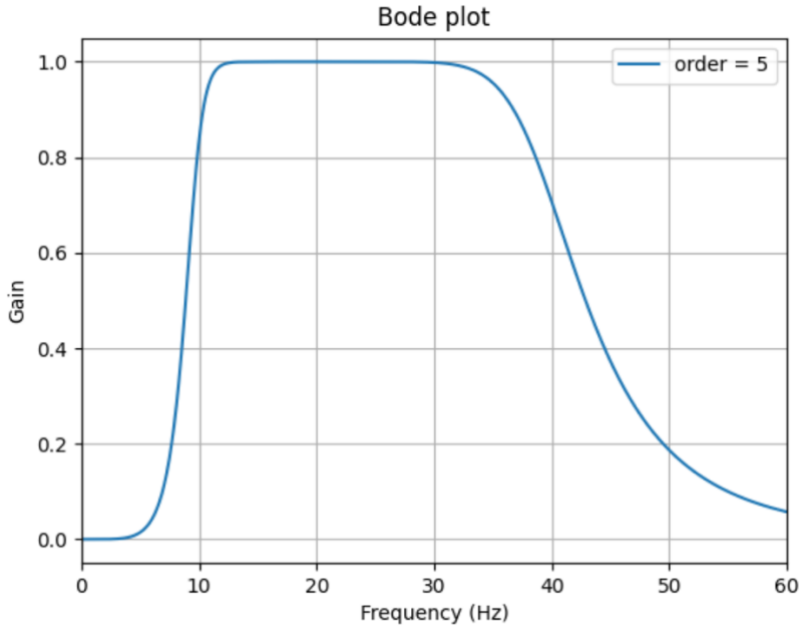

Figure 30. Bode Butterworth Bandpass Digital Filter of order 5.

Then when the signal was filtered, the temporal outliers were deleted, those samples which were higher than 9.1 were deleted from the buffer. This threshold of 9.1 was chosen with a testing of the different values, 9.1 was found to be the best relationship between deleting the outliers and conserving the high values. Because of the bandpass filter, no DC component was found on the signal on this point and so all the signals had an approximate mean of 0 and no offset this is a relevant aspect in order to delete the outliers correctly and to not miss delete some important signal. Finally, on the filtering part of the digital processing it was found that all the signals on the system had a very highly value on 11.5 Hz that is not related with any EEG event or stimulus, it was constant and the fact that it was so high lead to some highly error because of the alteration on the PSDA. Then the decision of making a Digital IIR Notch on this frequency was taken. It has been theorized by the author that some part of the electronic circuit added some important interference to the system. But no further investigation on the grounds has been made because the filter solved the problem.

It has been proved by testing that the logarithmic point of view works better than the linear, so at this point the transformation is made to the signal. Then some clearance of the signal is made inspired on the investigations [13] made. The PSDA was set to zero on the following intervals: (0, 8) Hz; (11.5, 13.5) Hz; (16.5, 18.5) Hz; (21.5, 28.5) Hz; (31, ∞) Hz. At this point, the signal was ready to the post-processing part.

Prediction Algorithms

There are several ways to detect which frequency is being observed, some of the methods are limited to the number of channels that are used, some others are limited by the spectral analysis.

This leads to an important concept of dimensionality, although the information is on the spectrum (choosing some frequency or the other), there is a need of having some information about the time dimension, because of the variant variable of decision over time (the subject might select one frequency at some instant and change to the other at the next moment).

This casuistry impedes the use of some classical frequency analysis such as Discrete Fourier Transform (DFT) or Fast Fourier Transform (FFT) which has high precision on the frequency domain but no precision on the time domain.

It is known by [14] that because of the Heisenberg's uncertainty principle, "*we can not measure simultaneously and with infinite precision a pair of conjugated magnitudes*", this means that is not possible to measure correctly and simultaneously both time and frequency domain. This principle can be understood easily on Figure 31.

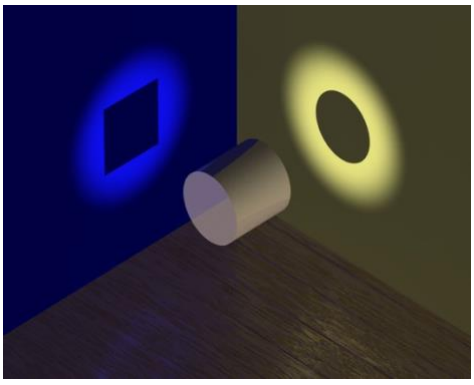

Figure 31. Easy representation of the Heisemberg's principle. [15]

It must be found a relationship between the time domain and the frequency domain. There are several options like the use of wavelets [14], [16], [17], [18], [19], [20] or the use of a deep learning neural network [21]. None of this method worked on the study case because of the lack of a bigger dataset to train the models.

An algorithm that do not need a large dataset is the widely used Canonical Correlation Analysis (CCA) [19], [22], [23], [24], [25], [26]. This method has been implemented and can be found on the Annex. It consisted on computing the correlation between a series of reference signals and the input signals, then for each reference signal there is one correlation coefficient, the greater coefficient between all the reference signal is the one considered to be the chosen one. This algorithm can be checked on Figure 32.

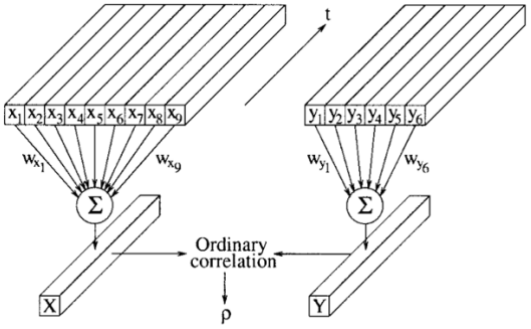

Figure 32. CCA Algorithm, where Xn are the different EEG channels and Yn are the signal reference and its harmonics. [22]

As it can be observed on Figure 32, the CCA algorithm works pretty well in one case: With more than one channel. In fact, as the number of channels increase the accuracy do so as [23] proved. The case study of the present project is done with only one channel and as [27] proved, new methods must be tried.

The next step was to try different predictive algorithms, such as Logistic regression [27] all the algorithms have high accuracy with recorded signals with the prototype (as it can be checked on Table 1).

Predictive Model	Accuracy
Logistic regression	78.9 %
Standard Vector Machine	78.9 %
Random Forest	77.48 %
KNN	75.43 %
Naive Bayes	73.12 %
AdaBoost	75.43 %
Decision Tree	68.79 %
MLP	77.46 %

Table 1. Accuracy of each predictive model on non-live measurements.

All of these algorithms do not work properly when evaluating the model with live features, the accuracy falls sharply to a point that is considered not to be acceptable. It has been theorized that the model training might be overfitting the small dataset.

Then the decision of choosing some features manually and classifying them with a self-made algorithm was made.

Feature extraction

The first feature that was extracted was the instant Signal to Noise Ratio (SNR) on the frequencies of interest, this is computed by taking the instant PSD on the frequency of interest (10 Hz or 15 Hz) and the mean of the PSD at the bandwidth near to the frequency by one Hertz, defined at Equation 7.

$$P_{instant_{SNR}}(f_{interest}) = \frac{PSD(f_{interest})}{PSD(f_{interest} - 1, f_{interest} + 1)}$$

Equation 7. Instant Power with the SNR.

Where $f_{interest} = 10\ Hz\ and\ f_{interest} = 15\ Hz$. Then, the higher value is stored as the first feature. The format of this feature is (0, 1), where 0 stands for the higher frequency being 10 Hz and 1 stands for the second frequency as the higher. As Equation 8 shows.

$$Feature_1 = index(\max\left(P_{instant_{SNR}}(10\ Hz), P_{instant_{SNR}}(15\ Hz)\right))$$

Equation 8. Selection of the first feature.

The same process is performed to the harmonics with the Equation 9.

$$P_{harmonic_{SNR}}(f_{harmonic}) = \frac{PSD(f_{harmonic})}{PSD(f_{harmonic} - 1, f_{harmonic} + 1)}$$

Equation 9. Power of the harmonic vs the SNR.

Where $f_{harmonic} = 2 * f_{interest}$, this is: $f_{harmonic} = 20\ Hz\ and\ f_{harmonic} = 30\ Hz$. The higher value of the two possibilities is stored as the second feature with the same format as the last feature. As equation 10 shows.

$$Feature_2 = index(\max\left(P_{harmonic_{SNR}}(20\ Hz), P_{instant_{SNR}}(30\ Hz)\right))$$

Equation 10. Selection of the second feature.

Then, the next feature that is saved is the instant PSDA, this feature is performed by obtaining the values of the PSDA at the frequency of interest and stores the index of the higher, thus the format is also (0, 1). As it can be checked on Equation 11.

$$Feature_3 = index(\max(PSD(10\ Hz), PSD(15\ Hz)))$$

Equation 11. Selection of the third feature.

Then the next feature is the harmonic value of PSD, like in feature 3, and as equation 12 shows.

$$Feature_4 = index(\max(PSD(20\ Hz), PSD(30\ Hz)))$$

Equation 12. Selection of the fourth feature.

Finally, the last feature that is considered is the power of the band of each stimulus frequency. This power is computed by integrating with the simpson's rule the PSD over the band of interest as follows at Equation 13.

$$Power_{band}(f_{interest}) = \int_{f_{interest}-1}^{f_{interest}+1} PSD(f)\, df$$

Equation 13. Power band on the frequency of interest.

Then, the feature is computed by extracting the higher value of the two possibilities as equation 14 shows.

$$Feature_5 = index(\max\left(Power_{band}(f_{interest_{10Hz}}), Power_{band}(f_{interest_{15Hz}})\right))$$

Equation 14. Selection of the fifth feature.

After the features extraction, several methods for the combination had been tested. The one that resulted with a high accuracy on the live feature classification was the calculus of the mode of all the features as follows on Equation 15.

$$Prediction = mode(Feature_1, Feature_2, Feature_3, Feature_4, Feature_5)$$

Equation 15. Final prediction with the mode.

Time Window

Once the algorithm is defined, it has been performed a study about the better window time that has to be used. In the bibliography [27], [28] among others, proved that the accuracy varies with the size of the time window of the signal, this variation can be checked on Figure X. These measures have been done on the case of 10 Hz and the case of 15 Hz, this is because it has been observed a different accuracy on all the methods depending on which objective is being observed. Moreover, on the aim of getting smaller windows, it has been found a problem on the purposed method because of a limitation on the calculations of PSD as it needs a minimum number of samples equals to the double of the sampling frequency.

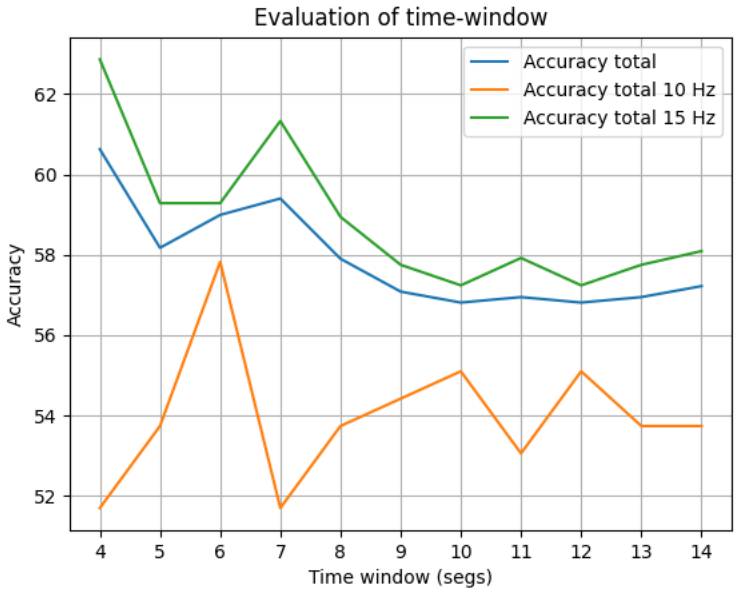

Figure 33. Accuracy vs time window, has been plotted with the annex "Fusion_Window_Test.py"

As Figure 33 shows, the greatest relationship is found at 6 seconds. This test has been performed with the previously recorded signals and as the purposed method is optimized for live features, the value of the accuracy is for guidance only on finding the best time window.

Design of the study

For this study a total of 4 different trials has been recorded, the testing study consisted of a relaxation time of 1 minute, then after it, a random succession (generated with a program for ensuring the randomness) of values are tell the user to stare each 7 seconds, this random succession is saved and the compared with the predicted values. Each match is count and divided by the number of total predictions, obtaining the accuracy of the system as Equation 16 shows, extracted from [29].

$$Accuracy = \frac{Correct\ predictions}{Total\ predictions} * 100$$

Equation 16. Accuracy formula.

Another standard measure on BCIs is the Information Transfer Rate (ITR) [30], this value represents the performance of a BCI that reflects both the amount of information transmitted per minute and the classification accuracy and speed per time unit. The formula (Equation 17) used on this case is the one used on [31].

$$ITR = B * S$$

Equation 17. ITR formula.

Where B (Equation 18) is the bit rate and S (Equation 19) is the speed of selection, thus,

$$B = \log_2 N + P(T) * \log_2 P(T) + (1 - P(T)) * \log_2(\frac{1 - P(T)}{N - 1})$$

Equation 18. Bit Rate formula

$$S = \frac{60}{T}$$

Equation 19. Speed of selection.

Where N is the number of possible selections, which in this project is two. And P is the average accuracy of the trials at a defined Time Window. The T on Equation X stands for the trial time which is 6 seconds.

These two methods of validation are the most used on every previously work done. [26], [31], [32], [33], [34].

On the exclusion criteria of the study, the head hair must be short.

Results

The main results of the different trials can be seen on the different columns on Table 2.

Series 1	Result 1	Series 2	Result 2	Series 3	Result 3	Series 4	Result 4
1	1	0	0	1	0	1	1
0	1	0	0	1	0	0	0
0	0	1	1	1	0	1	0
0	0	0	1	0	1	1	0
1	1	1	1	0	0	1	0
0	0	1	0	0	0	1	1
0	1	1	1	0	0	0	0
1	1	0	0	1	1	1	1
1	0	0	0	0	0	1	1

Table 2. General result of study.

The column called "Series" is the one generated randomly, while the "Result" column contains the predicted values during the acquisition. It is important to remember that the prediction is made each 6 seconds. As mentioned in methodology, the accuracy is computed using Equation 16.

And the results can be checked on Table 3.

	Trial 1	Trial 2	Trial 3	Trial 4
Correct Predictions	6	7	5	6
Total Predictions	9	9	9	9
Accuracy (%)	66,667	77,7778	55,5556	66,6667

Table 3. Statistics of the results.

Which leads to a total accuracy of 66.20 %, computed by doing the mean of all the trials. The total ITR computed with the Equation 17 is ITR = 9.07 bpm.

Discussion

Firstly, important results were obtained (in Table 1) using non-live signals, almost all the accuracies were on 70% which is the same result that Acampora obtained in [27], moreover, more predictive algorithm were tried and the result showed similar results like Acampora.

The results obtained on the live signals with the self-made new algorithm can be considered as valid because of the state of the art on the matter, it has to be taken into account that for a fair comparison, the other studies must be done with only one channel.

No study has done the full ecosystem (From hardware to software) so it has to be taken into account that most of the compared studies uses pre-made and high costs analog systems.

The only previously work on the field was made by Ronan Byrne on 2018 [3] that made the full analog system, but did not reach any result or prediction algorithm, so that is an improvement of the present project as the prediction algorithm was made and performed well.

Other papers that worked on a single channel BCI, were the Acampora's [27] method applying logistic regression, Lin's method using CCA [23] or Wangs method using PSDA [35].

All of the three mentioned previous worked, showed that for the limitation on the number of channels, the expected maximum accuracy is at 70%, while the minimum at 40%. As the accuracy obtained by the present project is 66% it has been considered a quite good result.
Moreover, all of them proved that a window size of approximately 6 seconds is considered to have the highest accuracy, as the present study proves.
Finally, most of the papers uses more than two objectives, this leads to having a not fair comparison of the ITR with any others, but having an ITR of 9.07 is considered valid as is in the normal value range [36].

Main conclusions

In conclusion, the main objective has been accomplished as the analog and digital system has been develop and validated for getting the correct prediction with an accuracy of 66%.
All the secondary objectives were fulfill as well, The signals were detected on the oscilloscope correctly, the one-channel EEG worked, the digitalization was achieved, the signal processing and feature extraction was made and then the prediction was also performed, finally the performance of the system was evaluated.

Secondary conclusions

A secondary conclusion that has been extracted is the fact that when generating the flickering objectives analogically with LEDs, a square-wave signal of the flickering frequency has to be generated with a function generator. Furthermore, it is known that the Fourier Series of a square-wave is a series of sinus of the frequency of the signal.
On the other side, the PSD of the SSVEP signal when cleaned, is also the summation of all the sinus components at the flickering frequencies.
Therefore, it can be concluded that in some way, it should be possible to reconstruct the original square-wave signal that had been generated.

This implies that the system could be considered an analogy of the optic fiber basis, where a LED blinks on a defined frequency and then is recorded by a photoresistor who turn the flashing lights on an electric signal again.

Another secondary conclusion found during the project is the fact that SSVEP proves something that might seem obvious but needs to be proved which is the fact that the environmental energy and frequencies can have an impact on the mind of humans.

Personal approach

During this project I have had the opportunity to immerse myself into the world of innovation by having to face and solve a lot of problems or drawbacks. The degree of freedom that I had was the most encouraging part, all the design decisions, or pathways… The field of neuroelectronic and the signal processing of the neural electrical activity has also been revealing for me, to the point of becoming my future steps on the professional field. I really think that this technology is going to be really evolved on the next years, and I hope I can do my bit to the cause.

Future Works

On the future works that can be done at the point of the projects are enormous. Firstly, I will be doing a PCB of the circuit and printing it. It should be done a validation on the system by comparing the results with a commercial EEG acquisition system. There is also the possibility of upgrading the algorithm with more robust prediction methods. Also, it can be tried to change the electrodes positions, or try to detect another neural signals…

I really think that a "generic manual for detecting biological electrical signals" could be made, because of the similarities on all the acquisition systems that has been observed.

Analogically, more channels could be add trying to have the smallest number of components.
It also could be tried to add more objectives…
Generally, this project field is more open now than ever, whichever idea does the engineer has, it should be tried and investigated.

I encourage anyone who find this field interesting to continue my work on it and upgrade my system with more ideas and innovations.

References

[1] A. Kawala-Sterniuk *et al.*, "brain sciences Summary of over Fifty Years with Brain-Computer Interfaces-A Review," 2021, doi: 10.3390/brainsci.

[2] René Descartes, "Discourse on Method," 1637.

[3] R. Byrne, "Development of a Low Cost, Open-source, Electroencephalograph-Based Brain-Computer Interface," 2018.

[4] Bit Brain, "Web Electrodes," https://www.bitbrain.com/blog/wet-eeg-cap.

[5] J. N. Acharya and V. J. Acharya, "Overview of EEG Montages and Principles of Localization," *J Clin Neurophysiol*, vol. 36, no. 5, p. 325—329, Sep. 2019, doi: 10.1097/wnp.0000000000000538.

[6] "Sistema 10/20," https://en.wikipedia.org/wiki/10%E2%80%9320_system_%28EEG%29.

[7] P. By ALLDATASHEETCOM, "OP27A, OP27C, OP27E, OP27G OP37A, OP37C, OP37E, OP37G LOW-NOISE HIGH-SPEED PRECISION OPERATIONAL AMPLIFIERS • Direct Replacements for PMI and LTC OP27 and OP37 Series Features of OP27A, OP27C, OP37A, and OP37C," 1989.

[8] B. Kibret, A. K. Teshome, and D. T. H. Lai, "Characterizing the human body as a monopole antenna," *IEEE Trans Antennas Propag*, vol. 63, no. 10, pp. 4384–4392, Oct. 2015, doi: 10.1109/TAP.2015.2456955.

[9] okawa-denshi, "LPF calculator," http://sim.okawa-denshi.jp/en/OPstool.php.

[10] "Active Notch Filter," https://www.electronics-notes.com/articles/analogue_circuits/operational-amplifier-op-amp/notch-filter-active-circuit.php.

[11] "Passive notch filter," https://medium.com/@electricaltechnology7233/notch-filter-theory-circuit-design-and-application-edd765204e50.

[12] Arduino, "Arduino MKR1010," https://store.arduino.cc/products/arduino-mkr-wifi-1010?gad_source=1&gclid=Cj0KCQjwj9-zBhDyARIsAERjds1GYmTvsuKq3inxcHqeztgfcM9HZ1jvgS-MqEenZ3S88XM-fc03o6IaAj06EALw_wcB.

[13] M. Cheng, X. Gao, S. Gao, and D. Xu, "Design and implementation of a brain-computer interface with high transfer rates," *IEEE Trans Biomed Eng*, vol. 49, no. 10, pp. 1181–1186, Oct. 2002, doi: 10.1109/TBME.2002.803536.

[14] V. J. Samar, A. Bopardikar, R. Rao, and K. Swartz, "Wavelet Analysis of Neuroelectric Waveforms: A Conceptual Tutorial," 1999. [Online]. Available: http://www.idealibrary.comon

[15] Juan García, "Principio de Incertidumbre de Heisenberg," https://www.hiberus.com/crecemos-contigo/principio-de-incertidumbre-de-heisenberg/.

[16] N. P. Castellanos and V. A. Makarov, "Recovering EEG brain signals: Artifact suppression with wavelet enhanced independent component analysis," *J*

Neurosci Methods, vol. 158, no. 2, pp. 300–312, Dec. 2006, doi: 10.1016/j.jneumeth.2006.05.033.
[17] W. Ting, Y. Guo-zheng, Y. Bang-hua, and S. Hong, "EEG feature extraction based on wavelet packet decomposition for brain computer interface," *Measurement (Lond)*, vol. 41, no. 6, pp. 618–625, Jul. 2008, doi: 10.1016/j.measurement.2007.07.007.
[18] "1P12-A guide for using the Wavelet Transform in Machine Learning – ML Fundamentals".
[19] P. Ma *et al.*, "A classification algorithm of an SSVEP brain-Computer interface based on CCA fusion wavelet coefficients," *J Neurosci Methods*, vol. 371, Apr. 2022, doi: 10.1016/j.jneumeth.2022.109502.
[20] P. Ma *et al.*, "An improved SSVEP Feature Extraction Algorithm Based on Multi-channel Wavelet Packet Coefficients and a Bayes Classifier," in *2021 6th International Conference on Signal and Image Processing, ICSIP 2021*, Institute of Electrical and Electronics Engineers Inc., 2021, pp. 154–158. doi: 10.1109/ICSIP52628.2021.9688997.
[21] O. Ozdamar, G. Zhu, S. Member, U. Yaylali, S. Member IEEE, and P. Jayakar, "Real-time Detection of EEG Spikes using Neural Networks."
[22] O. Friman, J. Cedefamn, P. Lundberg, M. Borga, and H. Knutsson, "Detection of Neural Activity in Functional MRI Using Canonical Correlation Analysis," 2001, doi: 10.1002/1522-2594(200102)45:2<323::AID-MRM1041>3.0.CO;2.
[23] Z. Lin, C. Zhang, W. Wu, and X. Gao, "Frequency recognition based on canonical correlation analysis for SSVEP-based BCIs," *IEEE Trans Biomed Eng*, vol. 53, no. 12, pp. 2610–2614, Dec. 2006, doi: 10.1109/TBME.2006.886577.
[24] Z. Lin, C. Zhang, W. Wu, and X. Gao, "Frequency recognition based on canonical correlation analysis for SSVEP-based BCIs," *IEEE Trans Biomed Eng*, vol. 53, no. 12, pp. 2610–2614, Dec. 2006, doi: 10.1109/TBME.2006.886577.
[25] M. Nakanishi, Y. Wang, Y. Te Wang, and T. P. Jung, "A comparison study of canonical correlation analysis based methods for detecting steady-state visual evoked potentials," *PLoS One*, vol. 10, no. 10, Oct. 2015, doi: 10.1371/journal.pone.0140703.
[26] M. Norizadeh Cherloo, H. Kashefi Amiri, and M. R. Daliri, "Spatio-Spectral CCA (SS-CCA): A novel approach for frequency recognition in SSVEP-based BCI," *J Neurosci Methods*, vol. 371, Apr. 2022, doi: 10.1016/j.jneumeth.2022.109499.
[27] Institute of Electrical and Electronics Engineers, *2019 IEEE International Conference on Systems, Man and Cybernetics (SMC) : Bari, Italy. October 6-9, 2019.*
[28] Institute of Electrical and Electronics Engineers, World Congress on Intelligent Control and Automation 11 2014.06.29-07.04 Shenyang, and WCICA 11 2014.06.29-07.04 Shenyang, *11th World Congress on Intelligent Control and Automation (WCICA), 2014 June 29, 2014 - July 4, 2014, Shenyang, China*.

[29] Evidently AI Team, "Accuracy on machine learning. ," https://www.evidentlyai.com/classification-metrics/accuracy-precision-recall.
[30] S. Sadeghi and A. Maleki, "Accurate estimation of information transfer rate based on symbol occurrence probability in brain-computer interfaces," *Biomed Signal Process Control*, vol. 54, Sep. 2019, doi: 10.1016/j.bspc.2019.101607.
[31] Institute of Electrical and Electronics Engineers, World Congress on Intelligent Control and Automation 11 2014.06.29-07.04 Shenyang, and WCICA 11 2014.06.29-07.04 Shenyang, *11th World Congress on Intelligent Control and Automation (WCICA), 2014 June 29, 2014 - July 4, 2014, Shenyang, China*.
[32] P. Ma *et al.*, "An improved SSVEP Feature Extraction Algorithm Based on Multi-channel Wavelet Packet Coefficients and a Bayes Classifier," in *2021 6th International Conference on Signal and Image Processing, ICSIP 2021*, Institute of Electrical and Electronics Engineers Inc., 2021, pp. 154–158. doi: 10.1109/ICSIP52628.2021.9688997.
[33] P. Ma *et al.*, "A classification algorithm of an SSVEP brain-Computer interface based on CCA fusion wavelet coefficients," *J Neurosci Methods*, vol. 371, Apr. 2022, doi: 10.1016/j.jneumeth.2022.109502.
[34] P. L. Lee, J. C. Hsieh, C. H. Wu, K. K. Shyu, and Y. Te Wu, "Brain computer interface using flash onset and offset visual evoked potentials," *Clinical Neurophysiology*, vol. 119, no. 3, pp. 605–616, Mar. 2008, doi: 10.1016/j.clinph.2007.11.013.
[35] Institute of Electrical and Electronics Engineers, World Congress on Intelligent Control and Automation 11 2014.06.29-07.04 Shenyang, and WCICA 11 2014.06.29-07.04 Shenyang, *11th World Congress on Intelligent Control and Automation (WCICA), 2014 June 29, 2014 - July 4, 2014, Shenyang, China*.
[36] W. Speier, C. Arnold, and N. Pouratian, "Evaluating True BCI Communication Rate through Mutual Information and Language Models," *PLoS One*, vol. 8, no. 10, Oct. 2013, doi: 10.1371/journal.pone.0078432.

Annex: